Liquid-metal plasma-facing component research on the National Spherical Torus Experiment

2013 Plasma Phys. Control. Fusion 55 124040

(http://iopscience.iop.org/0741-3335/55/12/124040)

Plasma Phys. Control. Fusion **55** (2013) 124040 (10pp) doi:10.1088/0741-3335/55/12/124040

Liquid-metal plasma-facing component research on the National Spherical Torus Experiment

M A Jaworski, A Khodak and R Kaita

Princeton Plasma Physics Laboratory, Princeton, NJ 08543, USA

E-mail: mjaworsk@pppl.gov

Received 12 July 2013, in final form 23 September 2013
Published 28 November 2013
Online at stacks.iop.org/PPCF/55/124040

Abstract

Liquid metal plasma-facing components (PFCs) have been proposed as a means of solving several problems facing the creation of economically viable fusion power reactors. Liquid metals face critical issues in three key areas: free-surface stability, material migration and demonstration of integrated scenarios. To date, few demonstrations exist of this approach in a diverted tokamak and we here provide an overview of such work on the National Spherical Torus Experiment (NSTX). The liquid lithium divertor (LLD) was installed and operated for the 2010 run campaign using evaporated coatings as the filling method. Despite a nominal liquid level exceeding the capillary structure and peak current densities into the PFCs exceeding 100 kA m^{-2}, no macroscopic ejection events were observed. The stability can be understood from a Rayleigh–Taylor instability analysis. Capillary restraint and thermal-hydraulic considerations lead to a proposed liquid-metal PFCs scheme of actively-supplied, capillary-restrained systems. Even with state-of-the-art cooling techniques, design studies indicate that the surface temperature with divertor-relevant heat fluxes will still reach temperatures above 700 °C. At this point, one would expect significant vapor production from a liquid leading to a continuously vapor-shielded regime. Such high-temperature liquid lithium PFCs may be possible on the basis of momentum-balance arguments.

(Some figures may appear in colour only in the online journal)

1. Introduction

Fusion energy holds the promise of nearly limitless, carbon-free energy. At present, however, there are significant unknowns as to whether fusion can ever be harnessed for commercial energy [1]. The uncertainties associated with the plasma-facing components (PFCs) and power extraction from these components are particularly acute. There is little hope of placing fusion energy within the pantheon of viable energy sources if this basic question cannot be answered: 'with what will one build the reactor?'

The present forerunner in reactor studies consists of PFCs composed of a solid refractory metal such as tungsten or its alloys [1, 2]. As recent reports point out, there are significant uncertainties as to whether tungsten will, ultimately extrapolate to an economically viable fusion reactor. Several failure modes exist that will force regular component replacements due to steady plasma loads and transient events. These have been highlighted in recent reports from CMOD and TEXTOR examining divertor and limiter operation when incident heat loads exceed the material limits of the PFC [3]. While these tests were failures under essentially steady loading, transient loading has long been known to cause melting and splashing of PFC surfaces when certain design criteria are exceeded. Simulated edge localized mode (ELM) damage in the QSPA plasma gun demonstrated tungsten target damage under ITER ELM-like energy loads [4]. Unmitigated ITER type-I ELMs are expected to deposit as much as 10 MJ m^{-2} onto the target and [4] suggests a limit of 1 MJ m^{-2} to eliminate damage and erosion to the PFCs. Recently, there is also evidence that a synergistic damage process occurs in PFCs subjected to a steady background pulses with additional transient loads (i.e. an environment similar to the divertor of a tokamak) [5]. These studies indicated that in the presence of a quasi-steady state plasma, ELM-like events that deposit

as little as $0.2\,\mathrm{MJ\,m^{-2}}$ will result in significant tungsten release from the PFC surface—fully five times less than limits suggested by previous plasma-gun experiments. These studies indicate a very low threshold energy for a given ELM to avoid damage which places significant demands on ELM-control and mitigation schemes. Even in the event that current research in ELM physics, control and mitigation could provide a solution, or in the event that an alternative configuration which, in principle, avoids all disruptions and transients altogether is utilized (e.g. stellarators), there are still steady-state processes that lead to permanent modification of the PFC surface.

The fusion PFCs in diverted machines are often classified as whether they are divertor PFCs or first-wall PFCs. While the plasma exhaust is focused in the divertor and faces the highest heat and particle fluxes, the first-wall is not devoid of interactions. In fact, there is a steady charge-exchange flux from the edge-plasma region impinging the first-wall PFCs [6]. Simple estimates of the erosion from the first-wall indicate net erosion rates on the order of several tons per year of tungsten [7]. This analysis already assumes that the divertor plasma is detached and in such a state that gross erosion is negligible in that area. Eroded material from the first-wall will be transported throughout the rest of the device by plasma processes and will eventually re-deposit in other locations. Studies of present-day machines already indicate net erosion from the first-walls of tokamak devices [8]. PFCs that continually thin will eventually require replacement—a prospect that carries negative economic implications for an eventual power reactor.

Liquid metal PFCs are a possible solution to the problem of plasma-reshaping of the PFC. Liquid metals exploit the fact that the natural progression of a heated metal is to liquefy and flow. This ability to flow the PFC material itself allows one to replenish the surface *in situ* and maintain an equilibrium PFC geometry by design. There are, however key issues that remain before a definitive answer on whether liquid metal PFCs are viable for use in a magnetized fusion energy device.

In this paper we will provide a discussion of three critical areas in liquid–metal PFC research: liquid metal stability, mass transport and material migration and integrated scenario development. Recent results in the NSTX with the liquid lithium divertor (LLD) indicate that the first of these issues can be addressed with suitable technologies and this analysis is provided below. The strategy for liquid metal stability suggests a certain concept for a liquid-metal PFC that is presented below: an actively-supplied, capillary-restrained system. Initial engineering studies of this concept already indicate the temperature range that such a PFC will operate (under fusion-relevant heat fluxes) and this has certain implications for future studies in confinement devices.

2. Key issues for liquid metal application to fusion devices

In 2004, DIII-D reported the results of the Li-DIMES experiments which showed macroscopic ejection of liquid lithium from the sample cup in that machine [9]. This result seemed to contrast the results from Russian experiments on the capillary porous systems in the T11-M device that did not exhibit ejection [10] nor were ejection events reported by the FTU device also using a capillary porous system [11]. Further tests in the CDX-U device with a large, free-surface limiter tray of liquid lithium also indicated stability [12]. This raised questions as to whether currents arising in the diverted configuration were destabilizing the liquid metal as T11-M, FTU and CDX-U were all limiter tokamaks. The first critical issue for liquid metals is to develop configurations and technologies that provide for stability of the free-surface in the face of steady and transient forces in the confinement device.

The second issue facing liquid metal PFCs is that of material mass balance. What is meant by this is that while the ability to replenish lost material at given surfaces is a key advantage for a liquid metal PFC, it is also a liability if an equal amount of material is not removed from locations of net deposition within the confinement device. Among the liquid metals often considered for use as a PFC (Li, Sn, Ga and alloys such as Sn–Li [13]), liquid lithium is known to have a strong chemical affinity for hydrogen, absorbing as much as 1 mole hydrogen per mole lithium to form LiH [14]. This affords a unique opportunity to control the hydrogenic inventory of a fusion device in that gettered material can be processed from the same stream of material supplied as the PFC surface. If the in-vessel inventory of the liquid lithium can be controlled, then the in-vessel inventory of tritium will also be controlled. This ability to flow liquid material in and out of a reactor is an important distinction between materials that absorb hydrogen that one might consider for use in a fusion reactor (i.e. carbon versus lithium). By the same token, this same gettering ability can become a significant liability for the usage of liquid lithium. Studies of the tritium balance in future reactors already indicate that the net quantity of tritium required on-site will depend critically on the amount trapped in the blanket and PFC system [15]. This, in-turn, places new demands on the overall tritium breeding ratio required of a sustainable reactor. Once a liquid-metal PFC can be deployed inside a tokamak, therefore, demonstration of mass-balance within the machine becomes a key technical demonstration for the concept overall.

The third issue facing liquid metal PFCs is that of finding an integrated scenario. Recent work on the JET-ILW project has again emphasized the importance of PFC material on core performance [16]. In particular, core performance was found to be sensitive to the operating scenario as some example discharges can exhibit tungsten core accumulation (with large core radiated power fractions) while others show H-factors of less than 0.9. ASDEX-Upgrade has been able to find scenarios with all-metal tungsten walls that exhibit good performance [17] and the question for each of the liquid metals is whether similar or better core performance can be achieved. At low temperatures liquid metals sputter and erode similar to solids, but exhibit temperature-enhanced sputtering at elevated temperature [18]. In addition to physical sputtering, evaporation can become significant at elevated temperatures. These elevated erosion rates can aid in power dissipation by providing a source of impurities to aid in radiative power dissipation—a large fraction of which is required for future

reactor schemes [19]. However, core contamination by those radiators must be minimized if fuel dilution (in the case of lithium) or radiative collapse (in the case of high-Z liquid metals) are to be avoided.

While all three of these issues are critical to addressing whether any particular liquid metal will be viable for future fusion devices, there is a particular priority in the first issue. If one is unable to produce a liquid-metal PFC that can be tested in a confinement device, then one cannot conduct the studies related to material migration nor integrated scenarios. Between the second two issues, finding a reactor-relevant scenario with high-confinement would then take precedence over material migration studies to avoid studying migration in a purely academic operating scenario. In this work we show that it is possible to develop stable liquid-metal PFCs for use in magnetic fusion devices as the first step to addressing the issues facing the concept in general.

3. Free-surface stability by capillary-restraint

The Rayleigh–Taylor instability provides a classic example of the formation of droplets from the interface of two fluids [20]. In this instability, a body force is acting upon two fluids such that the lighter fluid is supporting the heavier of the two. This configuration is unstable and the fluids tend to re-arrange themselves to the stable configuration where the heavier fluid is supporting the other. In the case of a liquid-metal PFC, the liquid metal represents the heavier fluid where vacuum or the plasma (effectively vacuum) provides the lighter fluid. The body force is supplied by gravity and currents flowing through the liquid metal interacting with the magnetic fields within the machine.

Currents through the liquid metal can be classified as steady or transient. Among the transient currents are those produced by disruptions [21] or ELMs [9]. Steady-state currents can arise from thermo-electric effects in the liquid-metal PFC itself [22], or scrape-off layer currents such as those driven by temperature differences between divertor legs [23]. Scrape-off layer current reversals have been observed in a number of machines and a continuous conductor would be expected to provide closure of the circuit [24]. These currents would flow parallel to the PFC surface in the poloidal plane and will interact with the toroidal magnetic field producing a $J \times B$ force normal to the PFC surface. It is this force that is considered below.

A derivation of the free-surface stability is given in [25]. In brief, the mass and momentum continuity equations for an incompressible fluid are given as follows:

$$\nabla \cdot \vec{u} = 0 \tag{1}$$

$$\rho\left(\frac{\partial \vec{u}}{\partial t} + (\vec{u}\cdot\nabla)\vec{u}\right) = \rho\vec{X} - \nabla p + \vec{J}\times\vec{B} + \mu_f \nabla^2\vec{u}, \tag{2}$$

where $\vec{u}$ is the fluid velocity, $\rho\vec{X}$ is a body force due to an acceleration such as gravity, g, pressure is indicated by p, $\vec{J}\times\vec{B}$ is the force arising from currents, $\vec{J}$, interacting with an imposed field, $\vec{B}$, and the final term in equation (2) is the dissipation due to viscosity, μ_f. In later equations the net body force due to external currents will be represented by the quantity, f. We assume a geometry where the fluid interface rests in the xy-plane and the imposed magnetic field is tangential to the surface in the x direction.

In the case of non-zero surface tension, Σ, acting at the fluid interface an additional term is applied as a boundary condition on the momentum equation [20]:

$$\Sigma\left(\frac{\partial^2}{\partial x^2} + \frac{\partial^2}{\partial y^2}\right)\delta z_s, \tag{3}$$

where δ is the Dirac delta function and z_s is the position of the interface. This term reflects the additional stress acting on the fluid due to the non-zero curvature and surface tension.

Normal modes are sought with the following form:

$$\exp(\mathrm{i}k_x x + \mathrm{i}k_y y + nt), \tag{4}$$

where $\mathrm{i} = \sqrt{-1}$, $k^2 = k_x^2 + k_y^2$ is the wave number of the disturbance with components in the x and y directions, and n is the growth rate (i.e. positive values of n indicate an unstable mode). After applying the analysis (see [25] for details) the following solution for the growth rate of an instability with wave number k for an inviscid fluid is found:

$$n^2 = k(g-f)\left[\frac{\rho_2-\rho_1}{\rho_2+\rho_1} - \frac{k^2\Sigma}{(g-f)(\rho_2+\rho_1)} - \frac{B^2k_x^2}{2\pi\mu_0(g-f)(\rho_2+\rho_1)k}\right]. \tag{5}$$

Equation (5) indicates several useful features. The first term indicates that the sum of accelerations g and f must result in an overall acceleration into the less-dense fluid, ρ_1, for an instability to occur. This is not sufficient, however, as the sum of terms in the square brackets $[\cdots]$ must also yield a net positive value (i.e. into the less-dense fluid) for the wave perturbation to be unstable. As we have begun the problem statement that $\rho_2 > \rho_1$, we can see the first term in the brackets is destabilizing due to the accelerations. The second term corresponds to the stabilizing force due to the surface tension of the fluid. (It is this term that causes small-diameter straws to retain a small amount of liquid after stirring a beverage). Finally, the effect of the magnetic field is similar to that of surface tension in that it provides stability, *but only for field-aligned wave vectors*. When one appropriately orients a perturbation at the fluid interface, the effect of the magnetic field can be nullified, even in the case of a perfectly conducting fluid. The effect of this stabilization varies with the wave number (i.e. the wavelength) such that more stability is provided the larger (smaller) the wavenumber (wavelength) of the perturbation.

Equation (5) can be re-arranged after solving for the marginal stability condition ($n = 0$). The least stable modes will be those that are aligned orthogonal to the applied field and only stabilized by the surface tension. In the case of the LLD, we consider a $\vec{J}\times\vec{B}$ force acting upward while gravity acts downward. We further consider $\rho = \rho_2 \gg \rho_1$, similar to a free-surface in contact with vacuum or a low-density plasma. One finds a critical wavenumber, k_{cr}, as follows:

$$k_{\mathrm{cr}} = \sqrt{\frac{jB-\rho g}{\Sigma}}. \tag{6}$$

Alternatively, a critical current density can be obtained as a function of wave length ($k = 2\pi/\lambda$):

$$j_{\mathrm{cr}} = \frac{1}{B}\left(\frac{4\pi^2}{\lambda^2}\Sigma + \rho g\right). \tag{7}$$

In equation (7) one can see the effect of reduced wavelength of the perturbation.

One can make use of geometry to enhance or eliminate the effects of surface tension. For example, surface texturing of tungsten or other metals can be used to enhance wicking of liquid metals up large vertical distances [26]. This same effect was exploited in the NSTX LLD.

Kelvin–Helmholtz type instabilities can also result in surface instabilities and waves and have been analyzed by several authors [27, 28]. In these works one finds that surface tension again plays a stabilizing role as does the magnetic field. Steady state flows are field-aligned in a tokamak divertor and this results in additional stabilization due to the presence of the magnetic field. This is predicted by analytical results to be stable, even for tungsten melt layers [28].

A cross-section of the NSTX vessel is shown in figure 1. The LLD was installed in the lower vessel at large major radius (0.65–0.85 m in machine coordinates) where high-triangularity, high-performance discharges could be run on conventional graphite PFCs and experiments could be conducted on the LLD surface in a single run campaign. The LLD consists of four 22 cm wide plates each having a toroidal extent of 82.5°. The quadrants are separated toroidally by graphite tiles that contain diagnostics and other instrumentation. The LLD plates are made of 2.2 cm thick copper with a 0.25 mm stainless-steel liner bonded to the surface. A flame-sprayed, porous molybdenum layer of approximately 0.15 mm thickness forms the plasma-facing surface on top of the stainless steel layer. Figure 2 shows images of the LLD hardware.

The LLD was intentionally installed to be slightly recessed of the adjacent graphite tiles. This was done to avoid any leading edges on the LLD itself which, by construction, only consisted of high-Z molybdenum on the front face whereas the side-walls consisted of a thin nickel plating over the stainless steel and copper bulk. The row of tiles inboard of the LLD are referred to as the 'bull-nose' tiles and extend from the LLD to the co-axial helicity injection (CHI) gap (62 cm).

Porous molybdenum is used for several reasons. The first of which is to provide a low sputter-yield material to cover the stainless steel layer on the LLD. Additionally, molybdenum is compatible with liquid lithium over the range of foreseeable temperatures in NSTX whereas previous studies have shown lithium can corrode stainless steel when contaminated with oxygen and nitrogen [29]. Finally, the porous molybdenum facilitates the wetting and subsequent spreading of liquid lithium over the LLD and also ensures that surface tension forces are large relative to electromagnetic forces to retain the liquid lithium during plasma operations [30].

The lithium capacity of the porous LLD surface was estimated to be 37 g via image analysis of cross-sectional micrographs of the flame-sprayed material. The 2010 experiments were performed with the LLD filled with

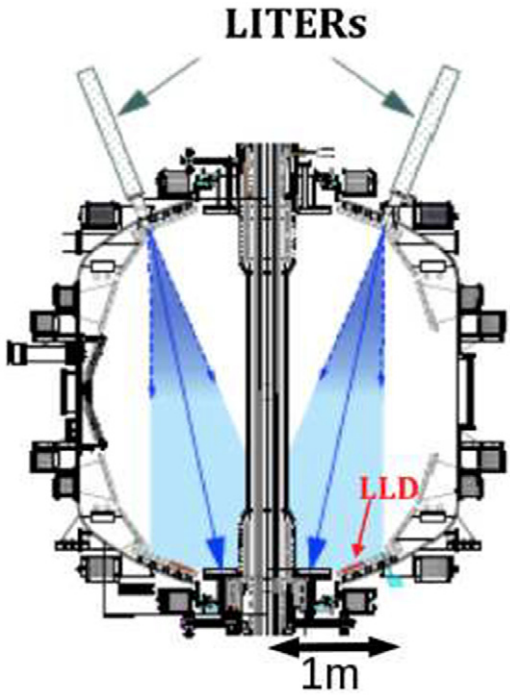

Figure 1. Cross-section of the NSTX vessel indicating location of the LLD installation in the lower vessel and LITER evaporation cones.

increasing amounts of deposited lithium, from a few percent at the beginning of the run campaign to an estimated 160% of fill on the last day of the run (60 g). Each of the four LLD segments included embedded electrical heaters and thermocouples for monitoring heating. The LLD was filled with lithium via the LITER evaporator system. Estimates place the filling efficiency of the LLD at about 7% of the total evaporated lithium [31]. By the end of the run campaign, therefore, approximately 860 g of lithium had been deposited into the machine, 60 g of which was located on the LLD plates themselves.

A new set of Langmuir probes in the high-density langmuir probe (HDLP) array were also implemented in the 2010 campaign and are located in one of the intersegment graphite diagnostic tiles. This probe array consists of 99 individual Langmuir probe tips arranged in a 3 × 33 pattern extending in radius from 62 to 72 cm in machine coordinates. More information on the HDLP can be found in the literature [32–34]. The surface temperature of the LLD was monitored with the use of dual-band infrared thermography [35]. Other diagnostics utilized include the typical suite of tools available on NSTX such as magnetic sensors (and associated EFIT reconstructions), divertor filter scopes and spectroscopy, and core measurements such as multi-point Thomson scattering and charge-exchange recombination spectroscopy.

The first notable results from operation with the LLD is that no molybdenum influx was observed during most discharges. As reported in [36], early in the run, when evaporations had been performed on the LLD while cold, molybdenum emission from the divertor was observed during MHD events. After reaching temperatures above the lithium melting point (181 °C), no such molybdenum emission was

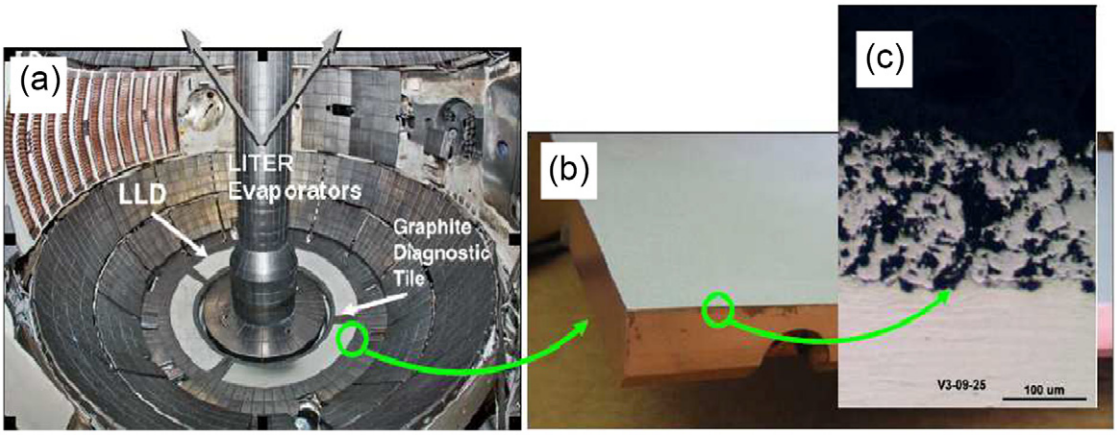

Figure 2. In-vessel hardware details of the LLD experiments. (*a*) shows the in-vessel installation of the LLD plates at the bottom of the vessel. (*b*) shows the LLD construction consisting of 2.2 cm copper substrate with bonded surface layers. (*c*) is a cross-sectional micrograph of the flame-sprayed, porous layer of molybdenum on top of the stainless-steel chemical barrier.

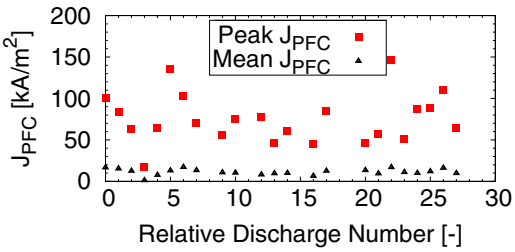

Figure 3. Quiescent and transient currents measured with the HDLP during a typical LLD run day. Each point represents an individual discharge where the mean current during the discharge is shown by the black triangles and the maximum value is shown by the red squares.

again observed. This repeats the results reported with the CPS devices which also indicated protection of the substrate material with liquid lithium [37].

The next notable result is that no macroscopic amounts of lithium were ejected from the LLD during the run campaign. Figure 3 shows a set of measurements of the current entering grounded PFCs during a typical run day as obtained with the HDLP. A typical quiescent current in the SOL of NSTX is at a level of 10 kA m^{-2}. Transient currents due to disruptions and ELMs can create currents entering the PFC an order of magnitude above the quiescent level. In the worst-case scenario, 100% of these currents will close across flux-surfaces through the PFC surface itself. This situation will result in the largest possible forces tending to destabilize the liquid.

Before the operating space of the LLD can be placed on a stability diagram, the expected wavelengths on the surface must be estimated. Scanning electron microscopy has been used on the porous, flame-sprayed molybdenum layer to generate an estimated pore size of $\approx 20\,\mu$m. An additional limit would be expected due to the depth of the fluid [30]. A conservative estimate on a droplet size limited by the fluid depth would place an upper-bound at about 100 μm. In the case of linear stability, then, the expected droplet sizes can be placed between $20 < r_{\text{droplet}} < 100\,\mu$m.

Figure 4 shows the marginal stability curve as a function of droplet radius for a number of magnetic fields. Also shown in the figure is the approximate operating space of the NSTX LLD as defined by the typical PFC currents measured during discharges and the estimated range of possible droplet radii. As can be seen, the NSTX LLD is predicted to be completely stable against Rayleigh–Taylor instabilities that might tend to eject droplets into the plasma. This is consistent with the lack of any observed ejection events. In the same figure, we make a comparison with results from the DIII-D Li-DIMES experiment which exhibited ejection of the lithium from a 25 mm diameter, 1 mm thick lithium sample at much lower injected current densities [9]. From the stability diagram, one can see that the Li-DIMES experiment is only marginally stable. The strategy of reducing pore size to stabilize a liquid metal was also implemented with the liquid lithium capillary porous system developed by Red Star [37]. In experiments in T11-M, it was found that by reducing the pore size of the mesh used in the CPS, droplet ejection could be eliminated. This usage of a porous substrate for stabilization of the free-surface liquid metal has now been demonstrated in a diverted tokamak.

In addition to the marginal stability analysis for liquid lithium, the same relations derived above should apply to other liquid metals of interest to the fusion community. In figure 4 is also shown the marginal stability curves for liquid tin under 2 or 5 T fields. This analysis indicates that similar porous structures as developed for liquid lithium systems should be applicable to liquid tin, provided certain conditions are met. These include chemical compatibility between the liquid metal and the porous material and sufficient wetting of the substrate by the liquid metal. This latter condition is particularly important as capillary pressure, $p_c \sim (\Sigma \cos\theta)/r_{\text{pore}}$, is directly proportional to the cosine of the contact angle, θ, between the liquid and the substrate. For contact angles approaching or exceed $\theta = \pi/2$, then, surface tension will have negligible effect in maintaining the adhesion of the liquid metal to the substrate. Provided such criteria are met, then the same techniques can be applied to stabilizing other liquid metals in a magnetic fusion device.

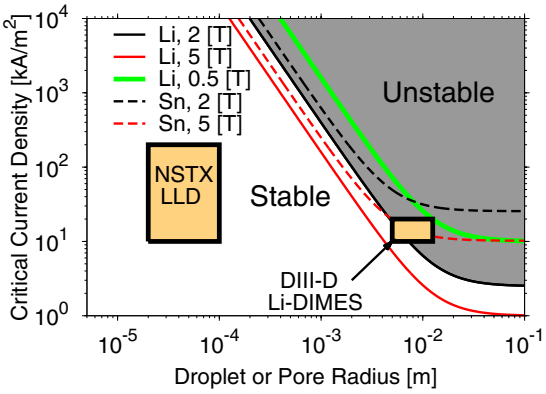

Figure 4. Stability diagram for a liquid metal under electromagnetic body forces (with gravity and surface tension stabilizing). NSTX LLD operating space indicated ($B_T = 0.5$ T). Comparison with Li-DIMES experimental space also shown ($B_T = 2$ T) [9]. No ejection events from the LLD were observed during the run campaign. Also shown in the figure are marginal stability curves for liquid tin.

Other notable results from the LLD experiments can be found in [25].

4. Design concept for a liquid metal PFC

Given the results above, certain design directions are suggested and here examined. First, it is seen that capillary forces can provide a powerful means of stabilizing a liquid metal against a number of forces. The objective of extracting power from the fusion plasma suggests some criteria based on thermal transport considerations. The simplest estimate for temperature rise, ΔT, through a material conducting heat is given as:

$$\Delta T \sim \frac{qL}{k_{\text{cond}}}, \tag{8}$$

where q is the incident heat flux, L is the thickness of the material and k_{cond} is the thermal conductivity of that material. For a given heat flux, then, the surface temperature can be reduced at the expense of material thickness. Both of these effects, capillary restraint and temperature rise, favor thinner materials and suggest an approach shown in figure 5 we refer to as 'actively-supplied, capillary-restrained systems' (ASCRS).

The basics of the concept are described here. Plasma is incident on the front face of the PFC providing heat to the surface as well as an erosion of the surface. Liquid metal is imbibed into the porous structure [38] and wets the surface to maintain a layer of liquid metal on top of the solid, textured substrate. Feed ports connect the front-face to a set of reservoirs for the liquid metal that are supplied from outside of the machine as well as provide a means of flowing material out. Closely coupled to the front-face of the structure are cooling pipes with some particular geometry that optimizes the efficacy of the coolant. The figure depicts an impinging jet scheme known as the 'T-tube' [39]. Other coolant schemes could be examined, but we consider this one as representative of the state-of-the-art in gaseous cooling technologies applicable to fusion PFCs.

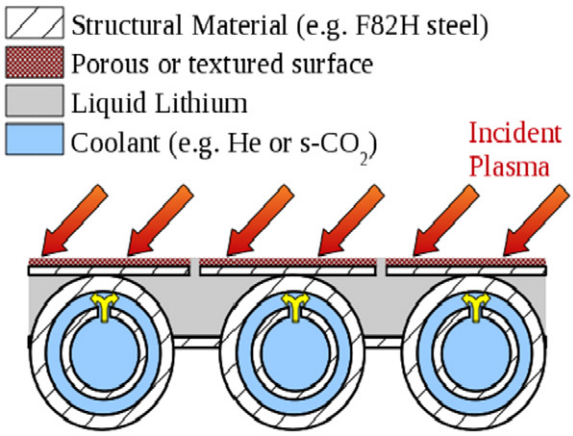

Figure 5. Schematic diagram of the actively-supplied, capillary-restrained systems. The basic concept features close-coupling of active coolant (here a T-tube scheme is shown), liquid metal reservoir (here liquid lithium), and a textured or porous front-face.

In the particular case of liquid lithium, a number of attractive features arise from such a concept. First, liquid lithium is chemically compatible with steels over a broad temperature range [29] (provided the oxygen and nitrogen contamination is controlled) whereas in the case of tin or gallium, only refractory metals are available for use (tin and gallium both corrode iron alloys at elevated temperatures) [40]. Provided temperature and stresses in the structure are compatible with the steel alloy used (see below), then this would eliminate the need to use tungsten in the PFC altogether. In this scheme, then, the liquid layer acts as a sacrificial material that can be eroded and replenished at will enabling thinner structures behind the front-surface. This thinning of the design does not negatively impact the life-time of the component as net reshaping of the PFC is completely eliminated (this feature would apply to the other liquid metals as well).

We have optimized the T-tube geometry for this particular application by taking advantage of the fact that the stress, σ_{pipe}, in the walls of a pressurized cylinder is given as follows:

$$\sigma_{\text{pipe}} = P\frac{R_{\text{pipe}}}{t_{\text{wall}}}, \tag{9}$$

where R_{pipe} is the pipe radius, P is the internal pressure and t_{wall} is the thickness of the pipe wall. Temperature across the wall of the pipe, by equation (9), is therefore proportional to t_{wall} which can be reduced at constant stress provided the radius of the pipe is also reduced by the same proportion. While in principle this reduction can be made to arbitrarily small pipe diameters, one must consider manufacturability of the structure as well.

An analysis of the thermal performance of such a system using the ANSYS-CFX commercial code is shown in figure 6. In this case, because the lithium is expected to be slowly flowing, it is possible to simulate the thermal transport throughout the lithium and steel as dominated by conduction and neglect convection through the metals [22]. Thermohydraulic modeling in this regime requires a turbulence

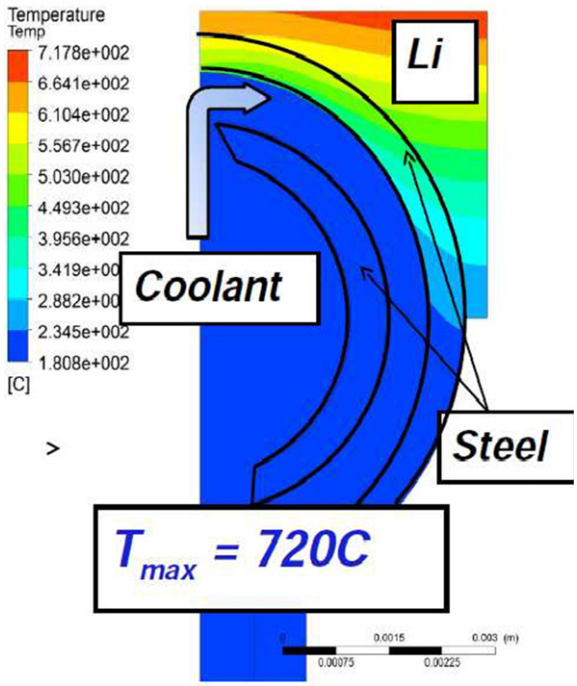

Figure 6. Thermal analysis of a modified T-tube system composed of steel and lithium with supercritical-CO_2 coolant. Heat flux is incident on the top of the simulation domain at a constant $10\,\mathrm{MW\,m^{-2}}$.

model to describe the gaseous coolant. A range of models exist and were examined in [39]. For the present study, the ANSYS/CFX code package was utilized which has its own implementations of the various turbulence models in common use in the fluid dynamics community. As the work reported in [39] included also some experimental validation of the turbulence model parameters used, the present study took pains to replicate the results reported in the earlier work. Once the simulations matched published data, the geometry and coolant type were modified in order to optimize for the liquid-metal application. In this case, we apply supercritical carbon-dioxide (CO_2) as the coolant due to a number of inherent advantages [41]. It is, of course, still possible to apply helium cooling as is typically done in fusion design studies. Details of the simulations supporting these design studies can be found in [42]. Surface temperatures above 720 °C are found in the 2D simulations using 180 °C inlet temperatures and a scaled geometry that maintains pipe-wall stresses below the yield strength of ODS-RAFM steels [43]. This will have significant implications on the operation of such a PFC in a tokamak divertor.

Alternative coolant schemes are also applicable to the ASCRS concept. We emphasize, again, that as the bulk of the thermal transport is dominated by conduction through the PFC, coolant schemes developed for solid-material PFCs are applicable provided they are compatible with the liquid metal used. In the current concepts, for instance, one would likely not utilize water-based coolant schemes with a liquid lithium-based PFC due to the exothermic reaction and release of hydrogen gas. However, in the case of liquid tin or gallium, such release of hydrogen gas does not occur, though rapid boiling and release of steam would still pose a hazard for such a system. Molten-salts are one option for a primary coolant. Molten salts were considered as a first-wall material instead of a liquid metal in the 'APEX' program [13]. While numerous free-surface studies were made, the use of the molten salt as a primary coolant is not discussed in that work. Typical drawbacks to the use of molten salts are the need to create highly turbulent flows to achieve effective cooling. The required pumping power for such high-speed flows would have to be assessed relative to the thermohydraulic performance of conventional gaseous cooling to determine if such a route is advantageous in this application. Another alternative to gaseous and liquid cooling is the use of heat pipes to redistribute the incident heat-flux [44]. Such devices still only conduct heat from one location to another and do not completely eliminate a fluid coolant scheme of some sort, but still represent a possible alternative to gaseous cooling. Even so, redistribution of the intense, divertor heat-flux reduces required peak heat flux at the next stage of cooling and so could result in reduced pumping powers overall. In the case of liquid metal heat-pipes, however, performance within magnetic fields still needs to be assessed for which the present research on porous metal PFCs is still somewhat applicable.

Previous studies of liquid lithium PFCs have focused on particle control aspects of the liquid lithium and the possibility of having strong retention leading to lowered recycling. Thermal desorption studies indicate that retention of hydrogen ceases above about 400 °C [14]. In addition, temperature-enhanced sputtering increases the yield from the surface but modeling of this effect suggests a saturation may be reached above 400 °C [18]. The largest effect will be an increase in the evaporative flux from the surface characterized in earlier studies [45]. The result for a high-temperature liquid lithium target would be to enter a regime that is high-recycling (similar to existing divertor targets) but one with a significant impurity fraction due to the ablating (i.e. sputtering and evaporating) lithium surface. We will refer to this regime as a *continuously vapor-shielded target*.

Knowing, then, that with fusion-divertor relevant heat fluxes, a vapor-shielded target can be expected, one must begin asking basic questions as to whether such a regime will be compatible with good core confinement. Previous studies have already indicated that vapor-shielding can effectively limit incident heat-fluxes during simulated ELM impacts [46], but this was an inherently transient study. Also, operation of the FTU tokamak has been successfully conducted above 550 °C [11], but this was with a liquid lithium *limiter*, not in a diverted configuration. One simple estimate is to consider momentum balance in a scrape-off layer flux tube.

The simplest estimate for momentum balance can be derived from the two-point model [47] which indicates that the upstream plasma pressure, p_u, equals the total pressure at the target given as:

$$p_u = p_t(1 + M^2) + p_n, \tag{10}$$

where p_t is plasma pressure at the target, M is the dynamic flow pressure (typically taken as $M = 1$) and p_n is the neutral pressure contribution. In the case of the vapor-shielded

target, this neutral pressure term could be considered to be dominated by the lithium vapor-pressure. One can see that in satisfying momentum balance that by increasing the lithium vapor-pressure one must decrease the plasma pressure on target to satisfy equation (10). This has the benefit of reducing the heat-load transmitted to the target from the plasma as the plasma heat flux, q_t^{plasma}, is given as follows [47]:

$$q_t^{\text{plasma}} = \gamma n_{se} c_s T_e = \gamma c_s p_t, \tag{11}$$

where γ is the sheath heat transmission coefficient, n_{se} is the density at the sheath edge, c_s is the sound speed and T_e is the temperature at the sheath edge. Reduction of the target plasma pressure therefore reduces the heat flux to the target due to the plasma.

Reduction of the incident plasma heat flux via pressure reduction is beneficial but not sufficient to completely describe the net result of a vapor-shielded regime. For this the full energy balance must be solved as, for example, the incident plasma energy may simply be transmitted to the neutral cloud and still be deposited upon the material target. This is the subject of on-going research. Radiated energy from the lithium vapor cloud should also be considered carefully as the cloud persists so close to the target that one may expect only $\approx 1/2$ of the energy to be emitted *away* from the target. A clear benefit can still be seen in reducing the plasma density in contact with the target in the form of reduced ionic fluxes. The charged species would otherwise be accelerated into the target and contribute to increased sputtering from target. It should be clear, however, that while the net energy balance remains to be examined, a liquid metal surface provides a replenishable surface that is self-healing. The usage of liquid lithium has the added benefit of being an impurity with a maximum $Z = 3$.

Typical target plasma pressures were measured in the NSTX LLD experiments and are shown in figure 7. Plasma pressure at the target was measured with the Langmuir probes for a range of powers crossing the last-closed flux surface, P_{SOL}, given as:

$$P_{SOL} = P_{NBI} + P_\Omega - P_{RAD} - \frac{dW}{dt}, \tag{12}$$

where P_{NBI} is the neutral beam heating power, P_Ω is the ohmic heating power, P_{RAD} is the radiative power loss and $\frac{dW}{dt}$ is the time-derivative of the stored energy in the plasma. We find that plasma pressures at the divertor target in the vicinity of the strike-point, p_t, averages about 100 Pa. Comparison with the lithium vapor pressure for a range of temperatures [48] indicates that a surface temperatures near 750 °C provide this pressure. This already indicates that at least the first criteria for momentum balance would not be violated for the temperatures calculated in figure 6 with the plasma pressures obtained in the divertor of the NSTX (i.e. that $p_n < p_u$ from equation (10)). Projecting ahead to the NSTX-U [49], we can estimate the upstream pressure in this machine using a relation found in [47] as follows:

$$P_{SOL} = 4\pi^2 R_0 a \kappa^{1/2} \frac{\chi_\perp}{\lambda_T} p_u, \tag{13}$$

where R_0, a and κ are the major radius, minor radius and elongation of the plasma respectively. $\chi_\perp$ is the cross-field

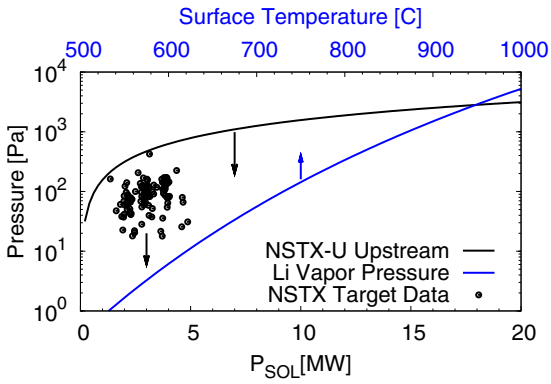

Figure 7. Comparison of typical plasma pressures in the NSTX divertor, predicted plasma pressure for the NSTX-U divertor and lithium vapor pressure over a range of surface temperatures.

thermal conductivity (here taken to be 2 $m^2\ s^{-1}$), and λ_T is the temperature gradient scale length in the SOL (estimated from heat-flux scaling length [50]). This scaling is also shown in figure 7 and indicates that a broad range of upstream pressures will be available when the upgrade comes online. At that time, integrated scenarios using such high-temperature, liquid lithium PFCs will be sought as well as assessments of the material migration throughout the machine.

5. Summary and conclusions

Plasma-facing components constructed of solid materials are presently the front-runner technology being considered for future devices. These components are, however, subject to net reshaping by plasma erosion, transport and redeposition. They are additionally vulnerable to transient loads that could cause melting and flow into new, undesired geometries. Liquid metal plasma-facing components provide an alternative approach which embraces the natural tendency of metals to melt and flow under intense heat loads. This technology has not been sufficiently developed, however, to definitively assess whether these materials will provide an acceptable material for a fusion reactor. Three key areas of research are indicated: establishing stable operation of the liquid-metal PFC within a fusion device, demonstrating control of the liquid metal inventory (and any absorbed materials such as tritium), and finally demonstrating an integrated scenario with good core confinement. The NSTX LLD experiments did not result in any ejection events into the plasma and this stability can be understood within the framework of the Rayleigh–Taylor instability.

Capillary-restraint and thermohydraulic considerations suggest one approach for liquid–metal plasma-facing components with the scheme of 'actively-supplied, capillary-restrained systems' or ASCRS. In the special case of a liquid lithium ASCRS, such a system would eliminate the need to use tungsten altogether. Initial assessments of the surface temperature of the ASCRS with divertor-relevant heat fluxes indicates the liquid lithium will generate a 'continuously vapor-shielded target'. An assessment of target plasma pressures in the divertor of NSTX indicate high-temperature lithium surfaces would not violate basic considerations of momentum

balance and the NSTX-U will be used to further assess these high-temperature, liquid lithium plasma-facing components to address the remaining critical issues listed above.

Acknowledgments

The authors would like to thank R Goldston and J Goh for many fruitful discussion in bringing forth the ASCRS concept. We also thank the NSTX Team for support installing and conducting experiments on the Liquid Lithium Divertor. This work supported by USDOE contracts DE-AC02-09CH11466.

References

[1] Zinkle S *et al* 2012 Materials science and technology research opportunities now and in the ITER era: a focused vision on compelling fusion nuclear science challenges *Technical Report* FESAC February 2012
[2] Phillips V 2011 Tungsten as material for plasma-facing components in fusion devices *J. Nucl. Mater.* **415** S2–9
[3] Coenen J W *et al* 2013 Evolution of surface melt-damage, its influence on plasma performance and prospects of recovery *J. Nucl. Mater.* **438** S27–33
[4] Federici G *et al* 2005 *J. Nucl. Mater.* **337–339** 684–90
[5] De Temmerman G *et al* 2011 ELM simulation experiments on Pilot-PSI using simultaneous high flux plasma and transient heat/particle source *Nucl. Fusion* **51** 073008
[6] Kotov V *et al* 2009 Numerical modelling of steady-state fluxes at the ITER first wall *J. Nucl. Mater.* **390–391** 528–31
[7] Stangeby P C 2011 Assessing material migration through ^{13}C injection experiments *J. Nucl. Mater.* **415** S278–83
[8] Hakola A *et al* 2013 Migration of impurities in fusion reactors: what have we learnt? *Plasma Phys. Control. Fusion* **55** 124029
[9] Whyte D G, Evans T E, Wong C P C, West W P, Bastasz R, Allain J P and Brooks J N 2004 Experimental observations of lithium as a plasma-facing surface in the DIII-D tokamak divertor *Fusion Eng. Des.* **72** 133–47
[10] Evtikhin V A, Lyublinski I E, Vertkov A V, Yezhov N I, Khripunov B I, Sotnikov S M, Mirnov S V and Petrov V B 2000 Energy removal and MHD performance of lithium capillary-pore system for divertor target application *Fusion Eng. Des.* **49–50** 195–9
[11] Apicella M L *et al* 2012 Lithization of the FTU tokamak with a critical amount of lithium injection *Plasma Phys. Control. Fusion* **54** 035001
[12] Majeski R *et al* 2003 CDX-U operation with a large area liquid lithium limiter *J. Nucl. Mater.* **313–316** 625–9
[13] Abdou M A and The APEX Team *et al* 2001 On the exploration of innovative concepts for fusion chamber technology *Fusion Eng. Des.* **54** 181–247
[14] Baldwin M J, Doerner R P, Luckhardt S C and Conn R W 2002 Deuterium retention in liquid lithium *Nucl. Fusion* **42** 1318–23
[15] Nishikawa M 2010 Study on tritium balance in a D–T fusion reactor *Fusion Sci. Technol.* **57** 120–8
[16] Beurskens M N A *et al* 2013 The effect of a metal wall on confinement in JET and ASDEX-upgrade *Plasma Phys. Control. Fusion* **55** 124043
[17] Dux R *et al* 2009 Plasma–wall interaction and plasma behaviour in the non-boronised all tungsten ASDEX upgrade. *J. Nucl. Mater.* **390–391** 858–63
[18] Allain J P *et al* 2003 Temperature dependence of liquid-lithium sputtering from oblique 700 eV He ions *J. Nucl. Mater.* **313–316** 641–5
[19] Kallenbach A *et al* 2013 Impurity seeding for tokamak power exhaust: from present devices via ITER to DEMO *Plasma Phys. Control. Fusion* **55** 124041
[20] Chandrasekhar S 1961 *Hydrodynamic and Hydromagnetic Stability* (New York: Dover)
[21] Gerhardt S P 2013 Dynamics of the disruption halo current toroidal asymmetry in NSTX *Nucl. Fusion* **53** 023005
[22] Jaworski M A, Morley N B and Ruzic D N 2009 Thermocapillary and thermoelectric effects in liquid lithium plasma facing components *J. Nucl. Mater.* **390–391** 1055–8
[23] Kumagai A *et al* 1997 Parallel currents in the scrape-off layer of high-density JT-60U discharges *Plasma Phys. Control. Fusion* **39** 1189–96
[24] Watkins J G *et al* 1997 Reciprocating and fixed probe measurements of density and temperature in the DIII-D divertor *J. Nucl. Mater.* **241–243** 645–9
[25] Jaworski M A *et al* 2013 Liquid lithium divertor characteristics and plasma-material interactions in NSTX high-performance plasmas *Nucl. Fusion* **53** 083032
[26] Lin T F *et al* 2013 Capillary wicking of liquid lithium on laser textured surfaces for plasma facing components *J. Nucl. Mater.* **433** 55–65
[27] Bazylev B, Landman I, Loarte A, Klimov N S, Podkovyrov V L and Safronov V M 2009 Experiments and modeling of droplet emission from tungsten under transient heat loads *Phys. Scr.* **T138** 014061
[28] Miloshevsky G and Hassanein A 2013 Splashing and boiling mechanisms of melt layer losses of PFCs during plasma instabilities *J. Nucl. Mater.* **438** S155–9
[29] Katsuta H *et al* 1977 *J. Nucl. Mater.* **71** 95–104
[30] Jaworski M A *et al* 2011 *J. Nucl. Mater.* **415** S985–8
[31] Kugel H W *et al* 2010 *Fusion Eng. Des.* **85** 865–73
[32] Kallman J, Jaworski M A, Kaita R, Kugel H and Gray T K 2010 High density Langmuir probe array for NSTX SOL measurements under lithiated divertor conditions *Rev. Sci. Instrum.* **81** 10E117
[33] Jaworski M A, Kallman J, Kaita R, Kugel H W, LeBlanc B, Marsala R and Ruzic D N 2010 Biasing, acquisition and interpretation of a dense Langmuir probe array in NSTX *Rev. Sci. Instrum.* **81** 10E130
[34] Jaworski M A *et al* 2012 Modification of the electron energy distribution function during lithium experiments on the national spherical torus experiment *Fusion Eng. Des.* **87** 1711–8
[35] McLean A G *et al* 2012 *Rev. Sci. Instrum.* **83** 053706
[36] Soukhanovskii V A *et al* 2010 *Rev. Sci. Instrum.* **81** 10D723
[37] Evtikhin V A *et al* 2002 Lithium divertor concept and results of supporting experiments *Plasma Phys. Control. Fusion* **44** 955–77
[38] Jaworski M A *et al* 2008 Observations of liquid lithium uptake in a porous molybdenum foam *J. Nucl. Mater.* **378** 105–9
[39] Abdel-Khalik S I *et al* 2008 Thermal-hydraulic studies in support of the ARIES-CS T-Tube divertor design *Fusion Sci. Technol.* **54** 864–77
[40] Zinkle S J and Ghoniem N M 2000 Operating temperature windows for fusion reactor structural materials *Fusion Eng. Des.* **51–52** 55–71
[41] Dostal V, Driscol M J and Hejzlar P 2004 A supercritical carbon dioxide cycle for next generation nuclear reactors *Technical Report* MIT-ANP-TR-100, MIT
[42] Khodak A and Jaworski M A 2013 Numerical analysis and optimization of divertor cooling system *Proc. SOFE (June)* vol 25 ThPO 45
[43] Zinkle S J *et al* 1998 Thermophysical and mechanical properties of Fe-(8-9)%Cr reduced activation steels *Technical Report* DOE/ER-0313/24, Oak Ridge National Laboratory p 135
[44] Makhankov A *et al* 1998 Liquid metal heat pipes for fusion application *Fusion Eng. Des.* **42** 373–9

[45] Doerner R P *et al* 2003 Behavior of high temperature liquid surfaces in contact with plasma *J. Nucl. Mater.* **313–316** 383–7
[46] Zhitlukhin A *et al* 2007 Effects of ELMs on ITER divertor armour materials *J. Nucl. Mater.* **363–365** 301–7
[47] Pitcher C S and Stangeby P C 1997 Experimental divertor physics *Plasma Phys. Control. Fusion* **39** 779–930
[48] Abdou M A *et al* 1999 On the exploration of innovative concepts for fusion chamber technology: APEX interim report *Technical Report* UCLA-ENG-99-206, University of California, Los Angeles
[49] Menard J E *et al* 2012 Overview of the physics and engineering design of NSTX upgrade *Nucl. Fusion* **52** 083015
[50] Makowski M A *et al* 2012 Analysis of a multi-machine database on divertor heat fluxes *Phys. Plasmas* **19** 056122